High-Fidelity Single-Qubit Gates on Neutral Atoms in a Two-Dimensional Magic-Intensity Optical Dipole Trap Array

Cheng Sheng,[1,2,3] Xiaodong He,[1,3,*] Peng Xu,[1,3] Ruijun Guo,[1,2,3] Kunpeng Wang,[1,2,3] Zongyuan Xiong,[1,3] Min Liu,[1,3] Jin Wang,[1,3] and Mingsheng Zhan[1,3,†]

[1]*State Key Laboratory of Magnetic Resonance and Atomic and Molecular Physics, Wuhan Institute of Physics and Mathematics, Chinese Academy of Sciences—Wuhan National Laboratory for Optoelectronics, Wuhan 430071, China*

[2]*School of Physics, University of Chinese Academy of Sciences, Beijing 100049, China*

[3]*Center for Cold Atom Physics, Chinese Academy of Sciences, Wuhan 430071, China*

(Received 18 December 2017; revised manuscript received 4 September 2018; published 10 December 2018)

As a conventional approach, optical dipole trap (ODT) arrays with linear polarization have been widely used to assemble neutral-atom qubits for building a quantum computer. However, due to the inherent scalar differential light shifts (DLS) of qubit states induced by trapping fields, the microwave-driven gates acting on single qubits suffer from errors on the order of 10^{-3}. Here, we construct a DLS compensated ODT array based upon a recently developed magic-intensity trapping technique. In such a magic-intensity optical dipole trap (MI-ODT) array, the detrimental effects of DLS are efficiently mitigated so that the performance of global microwave-driven Clifford gates is significantly improved. Experimentally, we achieve an average error of $(4.7 \pm 1.1) \times 10^{-5}$ per global gate, which is characterized by randomized benchmarking in a 4×4 MI-ODT array. Moreover, we experimentally study the correlation between the coherence time and gate errors in a single MI-ODT with an optimum error per gate of $(3.0 \pm 0.7) \times 10^{-5}$. Our demonstration shows that MI-ODT array is a versatile platform for building scalable quantum computers with neutral atoms.

DOI: 10.1103/PhysRevLett.121.240501

Neutral atoms in optical dipole trap (ODT) arrays, when serving as quantum bits (qubits), are believed to have outstanding scalability for quantum simulation and quantum computation [1–4]. Recently, atom-by-atom assemblers of defect-free one-dimensional (1D) and two-dimensional (2D) atomic arrays have been demonstrated and used to deterministically prepare 50 qubits [5,6]. Apart from the requirement of a sufficient qubit number, another ingredient of quantum computers is the high-fidelity performance of single-qubit and two-qubit gates in atom arrays. For single-qubit gates, two recent experiments provide a detailed characterization of microwave-driven single-qubit gate fidelities at Stark shift selected sites in 49-qubit 2D arrays and 125-qubit 3D arrays, respectively [7,8]. On the other hand, significantly improved fidelities of two-qubit quantum gates and entanglement have been achieved via the Rydberg blockade [9]. These achievements are important steps along the path of converting the scalability promise of neutral atoms into reality.

To perform fault-tolerant quantum computations via quantum error correction protocols, it requires that errors in quantum logic gates are small enough. Normally, the tolerable error varies among correction strategies, and the commonly accepted error threshold per gate is 10^{-4} [10–12]. Specifically, in neutral atom quantum computation architecture, single-qubit gates acting on qubits encoded in atomic hyperfine states can be implemented with microwave radiation [13] or with two-frequency Raman light [14]. Compared with Raman light, more stable and easily controlled microwave radiation, when used to drive qubit rotation, can suppress errors from laser-beam pointing instability and power fluctuations, and it can especially eliminate errors from spontaneous emission. It has already been used to implement single-qubit gates in a trapped ion qubit with errors of only 10^{-6}, far surpassing fault-tolerant thresholds [15]. In contrast to trapped ion qubits, microwave-driven gates on neutral atomic qubits undergo large errors, even without site addressing [7,8,16]. The achievement of microwave-driven gates with errors below 10^{-4} remains elusive [17]. Unlike ions, neutral atoms are optically trapped in ODT arrays. Because of the hyperfine structure splitting of several GHz, two states of a qubit experience a differential light shift (DLS) induced by the trapping laser fields. This DLS depends on the laser intensity seen by the qubits. Since there is a nonuniform spatial distribution of laser intensity over a trap volume, the qubits suffer from not only a strong inhomogeneous dephasing effect due to energy distribution of trapped atoms but also the homogeneous dephasing caused by the intensity fluctuations and the pointing instability of the ODT [18,19]. The former gives rise to an inhomogeneous broadening and leads to uncontrollable frequency detuning of up to over 100 Hz [7,8], and the latter limits the $1/e$ decay time denoted by T_{2s} of the spin-echo visibility

[16]. Combined with the relatively slow microwave-driven Rabi frequency (10 kHz, typically), all of the previously reported values of the average error per global microwave-driven gate in optically trapped qubit arrays are larger than 10^{-3} [7,8]. It is thus crucial to construct such an ODT array in which the detrimental DLS of qubits can be effectively compensated, so that one can implement high performance microwave-driven gates with errors per gate bellow 10^{-4}.

In order to make a "magic" trapping for the microwave clock transitions concerned, the working arrangement relies on applying a bias B field along a circularly polarized trapping laser field. In this manner, the trapping field induces a vector polarizability and a fourth-order hyperpolarizability. In the limit where the trapping fields are so weak that the hyperpolarizability can be neglected, the DLS of qubit states can be cancelled by setting a definite magnetic field with a given laser wavelength and degree of the circular polarization. This magic magnetic field technique has been demonstrated [20,21] and used to enhance the lifetime of quantum memory in a ^{87}Rb ensemble [22]. Until recently, it has been theoretically shown that, to consistently work out the magic trapping conditions for Cs atoms in optical traps, the term of hyperpolarizability cannot be neglected [23]. This higher order term makes the DLS dependence on the trapping laser intensity parabolic. Now the magic conditions are dependent on both the laser intensity and magnetic fields; i.e., for a given reasonable value of the B field, there exists such a definite intensity that the derivative of the DLS with respect to intensity equals zero; thus, the first order sensitivity of DLS to trapping light-intensity varied from whole ODT volume is eliminated and the inhomogeneous broadening is greatly suppressed. This laser intensity is called magic-intensity (MI), in contrast to the previous magic magnetic field. Experimentally, we measured the fourth-order hyperpolarizability contribution to the DLS of ^{87}Rb atoms and demonstrated that the coherence of a single mobile qubit is well preserved during a transfer process among two individual MI-ODTs [24]. The open question is whether this MI technique can be applied to promote the qualities of multiple qubits confined in an array and significantly improve the performance of microwave-drive gates. This question is explicitly answered in this Letter: across a 2D MI-ODT array, an average error of below 10^{-4} per global microwave-driven gate is obtained.

We begin by upgrading experimental setup for making a 2D MI-ODT array for confining ^{87}Rb atomic qubits. Subsequently, we improve the stability of the magnetic field to further enhance the coherence time of atomic qubits in the MI-ODT. Next, we perform randomized benchmarking (RB) experiments to characterize the fidelity of microwave-driven Clifford gates acting on single qubits in a single MI-ODT, and we study the correlation between the coherence time and average errors per gate. Then, we measure the uniformity and fidelity of global single-qubit gates in a 4×4 MI-ODT array. Finally, we discuss the potential for improving fidelity and crosstalk of site-selected single-qubit gates in a 2D MI-ODT array.

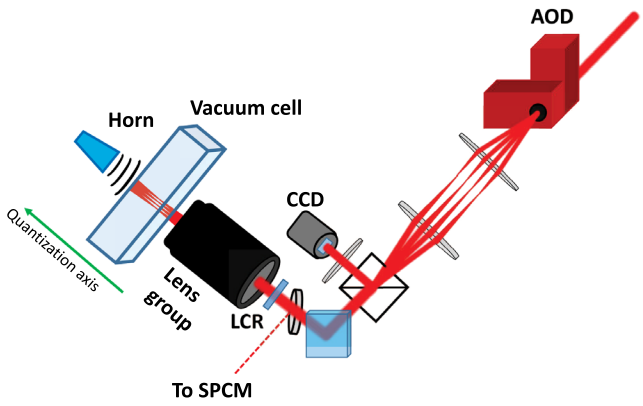

FIG. 1. Experimental setup for producing ODTs array. A 830 nm laser beam is deflected in two orthogonal directions to produce an ODT array by a dual-axis acousto-optic deflector (AOD) which is driven by a two-channel radio frequency (rf) with several tones. A liquid crystal retarder (LCR) is used to change the linearly polarized traps to circularly polarized magic-intensity traps. An objective lens not only provides a 3D tight confinement but also collects fluorescence from the trapped ^{87}Rb atoms. The fluorescence (denoted by dashed lines) is then counted by a single photon counting module (SPCM). A microwave horn external to the vacuum glass cell is used to deliver the microwave radiation.

Figure 1 illustrates the updated experimental setup for producing a 2D MI-ODT array. Driven by two-channel multitone radio-frequency (rf) signals, the dual-axis acousto-optic deflector (AOD) deflects a linearly polarized 830 nm laser beam into a 2D array of beams, each controlled by its own rf tone, which is similar to the work of generating a small array of OTD [25]. The output beam array is then focused to form a 2D ODT array, each with a waist of 1.0 μm. Limited by the availability of 830 nm laser power, we can only make a 4×4 ODT array such that trap depth of each site is deep enough to reliably load a single atom from the magneto-optical trap (MOT) [26], and the uniformity of the traps are within 12% after optimization [26]. We note that, as shown in Fig. 1, we use a single photon counting module (SPCM) instead of electron-multiplied-CCD camera (EMCCD) to detect the fluorescence of an individual, single atom. Certain single-site detection is realized by scanning the fluorescence image of the array together with spatial filtering techniques.

A physical qubit is encoded into microwave clock states of ^{87}Rb atom as $|0\rangle \equiv |F=1, m_F=0\rangle$ and $|1\rangle \equiv |F=2, m_F=0\rangle$. The MI-ODT and main experimental details on qubit preparation were described in Ref. [24]. In brief, we ultimately prepare single qubits with a temperature about 6–8 μK in a MI-ODT with a 41 μK trap depth. The single qubit is rotated by microwave radiation at a frequency about 6.834 GHz. Compared with our previous work [24], here we upgrade the microwave setup to satisfy

the requirements for precisely rotating the qubit [27]. With a microwave output of 1 Watt, the Rabi oscillation frequency is optimized up to about 12 kHz.

The magic-intensity trapping for ^{87}Rb atoms requires a magnetic field of several Gauss; thus, the qubit becomes sensitive to the noise of the magnetic field. With the working B field of 3.2 G, the homogenous dephasing from the magnetic field noise dominates the decay time of the Ramsey fringe in our previous experiments [24]. The coherence time T_{2s} was found to dominate the measurement error in neutral atomic qubits confined in an optical lattice [16]. To reduce the magnetic field noise and to obtain a longer T_{2s}, we choose to implement an active magnetic-field stabilization [28]. The resulting short-term stability is improved from 4 mG to sub-mG, measured by a flux-gate magnetometer. Consequently, the decay time of the Ramsey visibility is increased in the MI-ODT from $T_2 \approx 230(14)$ ms to $T_2 \approx 646(63)$ ms and T_{2s} can be extended to 1.72(8) s.

To characterize the errors of single-qubit gates driven by the microwave radiation, we adopt a well-developed RB method [30]. It has been proved to be a powerful technique that can distinguish gate errors from state preparation and measurement errors. We carry out the RB experiment by following the procedure described in Ref. [7]. In RB experiments, we use a complete set of 24 Clifford single-qubit gates C_1, which are generated from a set $\{\mathrm{I}, R_j(\pm\pi/2), R_j(\pi)\}$, where I is the identity gate and $R_j(\theta) = e^{-\imath\theta\sigma_j/2}$, with σ_j Pauli matrices about axes $j = x$, y, z. The basic spin rotations $R_j(\theta) = e^{-\imath\theta\sigma_j/2}$ are from precise control of the frequency, duration, and phase of microwave pulses. To precisely determine the qubit transition frequency and pulse durations, we perform two corresponding calibrations [31].

After preparing a qubit in $|0\rangle$ in the MI-ODT, random Clifford gate sequences of length ℓ, with each gate chosen from C_1, are implemented. At the end of each sequence, a final calculated Clifford gate is added and applied to bring the qubit state back to $|0\rangle$ with probability of 100% if the error is absent. As the length ℓ is increasing, the accumulated inevitable gate error reduces transfer fidelity, and the average probability of $|0\rangle$ state decays exponentially as [30]:

$$\bar{F} = \frac{1}{2} + \frac{1}{2}(1 - d_{if})(1 - 2\varepsilon_g)^{\ell}, \tag{1}$$

where d_{if} is the depolarization probability associated with state preparation and $|0\rangle$ read-out, while ε_g is the average error per Clifford gate. Thus, we can apply sequences of varying ℓ of randomized Clifford gates to single qubits initialized in $|0\rangle$ and fit the measured decay in an average $|0\rangle$ fidelity to Eq. (1) to obtain the values of d_{if} and ε_g.

In our experiments, we apply five different randomized Clifford gate sequences, each sequence is truncated at seven different lengths $\{1, 200, 400, 600, 800, 1000, 1300\}$. For every truncated length, each kind of sequence is implemented 300 times to obtain a probability in $|0\rangle$. The average fidelity of the randomized Clifford gate sequences at each truncation length is plotted in Fig. 2. A fit of these data to Eq. (1) yields an average error per gate of $\varepsilon_g \approx (3.0 \pm 0.7) \times 10^{-5}$ and $d_{if} \approx 0.03 \pm 0.01$. We note that, during the whole RB experiments, we do not regularly recalibrate the qubit transition frequency and the pulse durations.

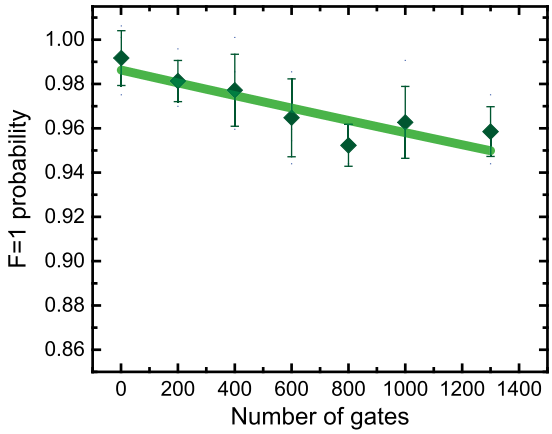

FIG. 2. Results of the single-qubit Clifford gate benchmarking experiment. The data are probabilities of measuring the $|0\rangle$ after applying five different random RB sequences truncated at different lengths $\ell = 1$, 200, 400, 600, 800, 1000, 1300. The closed points are the average values of five different RB sequences at each value of ℓ. Error bars are statistical, and represent the standard deviation of the mean. The solid line is a fit to Eq. (1), yielding, respectively, errors per gate of $\varepsilon_g \approx (3.0 \pm 0.7) \times 10^{-5}$ and state preparation errors and readouts errors $d_{if} \approx 0.03 \pm 0.01$.

To understand the sources contributing to the above measured error per gate, we examine three main sources of error during the RB experiment: (1) frequency detuning from the qubit transition, (2) fluctuations of $\pi/2$ pulse area, (3) qubit dephasing. For the detailed processes, see [32].

Apart from the above two minor effects, the dephasing contributing error can be roughly estimated by taking the ratio of our qubits coherence time of $T_{2s} \approx 1.72$ s to the average gate time of 75.73 μs, yielding an error per gate of 4.4×10^{-5}, which is larger than the measured value. This disagreement suggests that the phase noise of qubits measured by the spin-echo experiment is larger than the one at a short time scale, relevant to the single-qubit gate [33], since the spin-echo experiments measure the decay of phase coherence for large magnitudes over long time scales. We define a characteristic coherence time T_{RB} to describe the phase noise at a short time scale relevant to the RB experiment, and we assume that a ratio of T_{RB} to T_{2s} is η.

To determine η in the RB experiment, we measure the dependence of errors ε_g on coherence time T_{2s}, as shown in

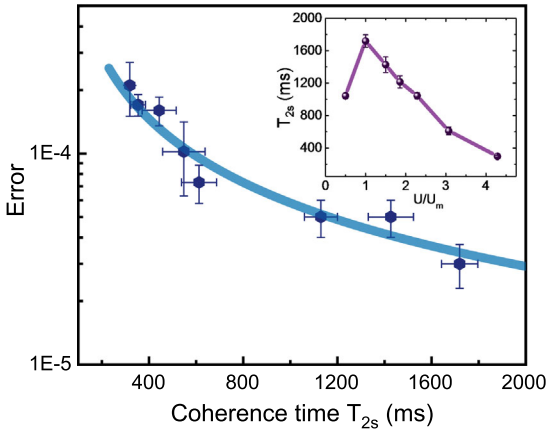

FIG. 3. Dependence of values of errors per gate on the coherence times T_{2s}. All values of errors per gate are measured by using the RB method. All of the accompanying error bars of coherence times and the values of errors per gate are fitting errors. The solid curve is fit to Eq. (2). The inset shows the dependence of coherence time T_{2s} on the ratio of varied trap depths (U) to magic working trap depth (U_m). The accompanying solid curve is to guide the eye.

Fig. 3. Here, the coherence time T_{2s} is scanned by increasing the laser intensity of the ODT. Because of the parabolic intensity dependence of light shifts in a circularly polarized ODT, atoms experience a more homogeneous dephasing effect when the working intensity is away from the magic point, as illustrated by the solid curves in the inset of Fig. 3. We can immediately see that under the same experimental conditions including a control pulse duration, noise fluctuations of the magnetic field and microwave power, the error obviously increases as the coherence time reduces. Neglecting the contribution of the pulse area error to the total measured errors, the ε_g is given by

$$\varepsilon_g(T_{2s}) = 1 - e^{-t_{CG}/\eta * T_{2s}}, \tag{2}$$

where $t_{CG} \approx 75.73\ \mu$s is the average time duration of Clifford gates, including an idle time of 3 μs. A fit to Eq. (2) yields $\eta \approx (1.30 \pm 0.07)$. From the fitting, we can see that in our experiments, the short period phase noise can be scaled to the coherence time T_{2s}, and it dominates the error per gate. This result is qualitatively in agreement with the one shown in the previous experiment done in a linearly polarized optical lattice [16]. Taking account of the trap inhomogeneity of 12% across the array and the relationship shown in Fig. 3, it is expected that high fidelity microwave-driven gates across the MI-ODT array can be achieved.

Now we carry out the array experiments. Since we are using a SPCM for fluorescence detection, we characterize the average errors per global gate across the MI-ODT array site by site. The sequence of site-by-site scanning is shown in Fig. 4(a), which is indicated by the arrows. For each site labeled, we carry out RB experiments and obtain the

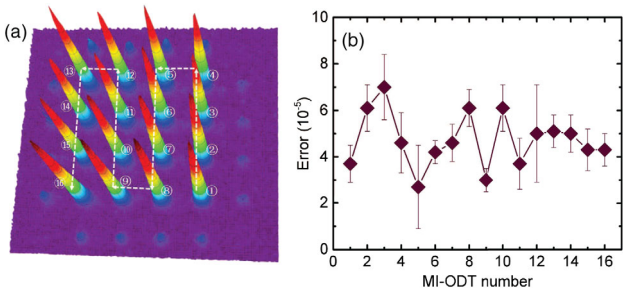

FIG. 4. Array experiments. (a) Measurement sequence. Specifically, each site of the array is labeled from 1 to 16. The dashed arrows indicate the path of scanning. (b) The recorded values of error per gate as a function of site number. All values of error per gate are measured by using RB method. All the accompanying error bars error per gate are fitting errors. The lowest and highest gate errors are $(2.7 \pm 1.8) \times 10^{-5}$ and $(7.0 \pm 1.4) \times 10^{-5}$ respectively.

results, which are similar to those shown in Fig. 2, from which the corresponding average errors per gate is extracted as a data point plotted in Fig. 4(b). To ensure the consistency of Clifford gates, the frequency and pulse durations of the RB pulses remain unchanged throughout the experiment. After completing the experiment, the measured errors per gate, as a function of the site number, are plotted in Fig. 4(b). By averaging all of the 16 points of data, ranging from $(2.7 \pm 1.8) \times 10^{-5}$ to $(7.0 \pm 1.4) \times 10^{-5}$, an average error of $(4.7 \pm 1.1) \times 10^{-5}$ per gate is obtained. Since the microwave is passively stabilized and the measurements normally take two weeks, there is inevitably a drift in the microwave power in this long-term measurement. According to the numerical estimation, a change of 0.3% in pulse length during the experiments will lead to an error per gate of about 3×10^{-5}. Therefore, the fluctuations of the $\pi/2$ pulse area would largely cause fluctuations in errors per gate during the site-by-site measurements, as shown in Fig. 4(b). Other trivial factors related to the inhomogeneity of fidelities are of the inhomogeneous spatial distribution of microwave power and the gradient of the magnetic field, but for such a tiny scale of MI-ODT arrays, these factors could be neglected. We anticipate that the results will be more uniform if the RB experiments are carried out with defect-free 2D atomic arrays and measured in parallel using a camera for the detection of fluorescence.

By the above results, we demonstrated the novel feature of a MI-ODT array in improving the fidelity of microwave-driven gates acting on single qubits. The improvement is based on the fact that in MI-ODT the DLS is largely eliminated so that the accuracy of the microwave operation is manifested. This feature could also be beneficial to low cross talk single-qubit gates if we use an addressing method like targeted phase shifts originally devised in Ref. [8], since in that experiment, the largest contributions to errors per gate on target qubits and cross talk on spectator atoms are both from the global microwave error.

In summary, we have experimentally proved that the MI-ODT array can greatly promote the qualities of multiple qubits and significantly improve the performance of microwave-driven gates with errors below 10^{-4} for fault-tolerance. An average gates error of $(4.7 \pm 1.1) \times 10^{-5}$ is achieved across the MI-ODT array. Our presently obtained single-qubit gate fidelity is already slightly higher than the one in the nitrogen vacancy center qubit [34], and it is substantially higher than the ones in superconducting qubits [35] and quantum dots [36]. Compared with the currently used high performance magnetic shield, the realization of the doubly magic trapping, proposed by Carr and Saffman [23], is a more attractive route to obtaining insensitivity to the magnetic field noise. We anticipate that with sufficient improvements in magnetic field noise, a level of performance of single-qubit gates that has already been demonstrated with trapped ion hyperfine qubits [15] will also become feasible for optically trapped neutral atoms. This work, together with our previous demonstration of the coherent transfer of a mobile qubit [24] and the entanglement of two individual atoms of different isotopes (^{87}Rb and ^{85}Rb) via Rydberg blockade [37], represents key steps towards a scalable quantum computer with neutral atoms trapped in MI-ODT arrays.

We acknowledge fruitful discussions with M. Saffman, T. Xia, and A. Derevianko. This work was supported by the National Key Research and Development Program of China under Grants No. 2017YFA0304501, No. 2016YFA0302800, and No. 2016YFA0302002, the National Natural Science Foundation of China under Grant No. 11774389, and the Strategic Priority Research Program of the Chinese Academy of Sciences under Grant No. XDB21010100.

*hexd@wipm.ac.cn
†mszhan@wipm.ac.cn

[1] H. Bernien, S. Schwartz, A. Keesling, H. Levine, A. Omran, H. Pichler, S. Choi, A. S. Zibrov, M. Endres, M. Greiner, V. Vuletić, and M. D. Lukin, Probing many-body dynamics on a 51-atom quantum simulator, Nature (London) **551**, 579 (2017).

[2] M. Saffman, T. G. Walker, and K. Mölmer, Quantum information with Rydberg atoms, Rev. Mod. Phys. **82**, 2313 (2010).

[3] I. M. Georgescu, S. Ashhab, and F. Nori, Quantum simulation, Rev. Mod. Phys. **86**, 153 (2014).

[4] D. S. Weiss and M. Saffman, Quantum computing with neutral atoms, Phys. Today **70**, No. 7, 44 (2017).

[5] M. Endres, H. Bernien, A. Keesling, H. Levine, E. R. Anschuetz, A. Krajenbrink, C. Senko, V. Vuletic, M. Greiner, and M. D. Lukin, Atom-by-atom assembly of defect-free one-dimensional cold atom arrays, Science **354**, 1024 (2016).

[6] D. Barredo, S. Léséleuc, V. Lienhard, T. Lahaye, and A. Browaeys, An atom-by-atom assembler of defect-free arbitrary two-dimensional atomic arrays, Science **354**, 1021 (2016).

[7] T. Xia, M. Lichtman, K. Maller, A. W. Carr, M. J. Piotrowicz, L. Isenhower, and M. Saffman, Randomized Benchmarking of Single-Qubit Gates in a 2D Array of Neutral-Atom Qubits, Phys. Rev. Lett. **114**, 100503 (2015).

[8] Y. Wang, A. Kumar, T. Wu, and D. S. Weiss, Single-qubit gates based on targeted phase shifts in a 3D neutral atom array, Science **352**, 1562 (2016).

[9] H. Levine, A. Keesling, A. Omran, H. Bernien, S. Schwartz, A. S. Zibrov, M. Endres, M. Greiner, V. Vuletć, and M. D. Lukin, High-Fidelity Control and Entanglement of Rydberg Atom Qubits, Phys. Rev. Lett. **121**, 123603 (2018).

[10] E. Knill, Quantum computing with realistically noisy devices, Nature (London) **434**, 39 (2005).

[11] A. M. Steane, Error Correcting Codes in Quantum Theory, Phys. Rev. Lett. **77**, 793 (1996).

[12] S. J. Devitt, W. J. Munro, and K. Nemoto, Quantum error correction for beginners, Rep. Prog. Phys. **76**, 076001 (2013).

[13] D. Schrader, I. Dotsenko, M. Khudaverdyan, Y. Miroshnychenko, A. Rauschenbeutel, and D. Meschede, Neutral Atom Quantum Register, Phys. Rev. Lett. **93**, 150501 (2004).

[14] S. Yu, P. Xu, M. Liu, X. D. He, J. Wang, and M. S. Zhan, Qubit fidelity of a single atom transferred among the sites of a ring optical lattice, Phys. Rev. A **90**, 062335 (2014).

[15] T. P. Harty, D. T. C. Allcock, C. J. Ballance, L. Guidoni, H. A. Janacek, N. M. Linke, D. N. Stacey, and D. M. Lucas, High-Fidelity Preparation, Gates, Memory, and Readout of a Trapped-Ion Quantum Bit, Phys. Rev. Lett. **113**, 220501 (2014).

[16] S. Olmschenk, R. Chicireanu, K. D. Nelson, and J. V. Porto, Randomized benchmarking of atomic qubits in an optical lattice, New J. Phys. **12**, 113007 (2010).

[17] M. Saffman, Quantum computing with atomic qubits and Rydberg interactions: Progress and challenges, J. Phys. B **49**, 202001 (2016).

[18] S. Kuhr, W. Alt, D. Schrader, I. Dotsenko, Y. Miroshnychenko, A. Rauschenbeutel, and D. Meschede, Analysis of dephasing mechanisms in a standing-wave dipole trap, Phys. Rev. A **72**, 023406 (2005).

[19] S. Yu, P. Xu, X. D. He, M. Liu, J. Wang, and M. S. Zhan, Suppressing phase decoherence of a single atom qubit with Carr-Purcell-Meiboom-Gill sequence, Opt. Express **21**, 32130 (2013).

[20] N. Lundblad, M. Schlosser, and J. V. Porto, Experimental observation of magic-wavelength behavior of ^{87}Rb atoms in an optical lattice, Phys. Rev. A **81**, 031611 (2010).

[21] A. Derevianko, Theory of magic optical traps for Zeeman-insensitive clock transitions in alkali-metal atoms, Phys. Rev. A **81**, 051606 (2010).

[22] Y. O. Dudin, R. Zhao, T. A. B. Kennedy, and A. Kuzmich, Light storage in a magnetically dressed optical lattice, Phys. Rev. A **81**, 041805 (2010).

[23] A. W. Carr and M. Saffman, Doubly Magic Trapping for Cs Atom Hyperfine Clock Transitions, Phys. Rev. Lett. **117**, 150801 (2016).

[24] J. Yang, X. D. He, R. J. Guo, P. Xu, K. P. Wang, C. Sheng, M. Liu, J. Wang, A. Derevianko, and M. S. Zhan, Coherence

Preservation of a Single Neutral Atom Qubit Transferred Between Magic-Intensity Optical Traps, Phys. Rev. Lett. **117**, 123201 (2016).

[25] B. J. Lester, N. Luick, A. M. Kaufman, C. M. Reynolds, and C. A. Regal, Rapid Production of Uniformly Filled Arrays of Neutral Atoms, Phys. Rev. Lett. **115**, 073003 (2015).

[26] See Supplemental Material at http://link.aps.org/supplemental/10.1103/PhysRevLett.121.240501 for a discussion of generating and optimizing ODT arrays, which includes Ref. [5].

[27] See Supplemental Material at http://link.aps.org/supplemental/10.1103/PhysRevLett.121.240501 for a discussion of the upgraded microwave system.

[28] See Supplemental Material at http://link.aps.org/supplemental/10.1103/PhysRevLett.121.240501 for a discussion of actively stabilizing magnetic field, which includes Ref. [29].

[29] C. J. Dedman, R. G. Dall, L. J. Byron, and A. G. Truscott, Active cancellation of stray magnetic fields in a Bose-Einstein condensation experiment, Rev. Sci. Instrum. **78**, 024703 (2007).

[30] E. Knill, D. Leibfried, R. Reichle, J. Britton, R. B. Blakestad, J. D. Jost, C. Langer, R. Ozeri, S. Seidelin, and D. J. Wineland, Randomized benchmarking of quantum gates, Phys. Rev. A **77**, 012307 (2008).

[31] See Supplemental Material at http://link.aps.org/supplemental/10.1103/PhysRevLett.121.240501 for a discussion of calibrating the microwave pulse length and frequency.

[32] See Supplemental Material at http://link.aps.org/supplemental/10.1103/PhysRevLett.121.240501 for a discussion of main error sources during RB experiment.

[33] K. R. Brown, A. C. Wilson, Y. Colombe, C. Ospelkaus, A. M. Meier, E. Knill, D. Leibfried, and D. J. Wineland, Single-qubit-gate error below 10^{-4} in a trapped ion, Phys. Rev. A **84**, 030303(R) (2011).

[34] X. Rong, J. P. Geng, F. Z. Shi, Y. Liu, K. B. Xu, W. C. Ma, F. Kong, Z. Jiang, Y. Wu, and J. F. Du, Experimental fault-tolerant universal quantum gates with solid-state spins under ambient conditions, Nat. Commun. **6**, 8748 (2015).

[35] R. Barends, J. Kelly, A. Megrant, A. Veitia, D. Sank, E. Jeffrey, T. C. White, J. Mutus, A. G. Fowler, B. Campbell, Y. Chen, Z. Chen, B. Chiaro, A. Dunsworth, C. Neill, P. OMalley, P. Roushan, A. Vainsencher, J. Wenner, A. N. Korotkov, A. N. Cleland, and J. M. Martinis, Superconducting quantum circuits at the surface code threshold for fault tolerance, Nature (London) **508**, 500 (2014).

[36] M. Veldhorst, J. C. Hwang, C. H. Yang, A. W. Leenstra, B. de Ronde, J. P. Dehollain, J. T. Muhonen, F. E. Hudson, K. M. Itoh, A. Morello, and A. S. Dzurak, An addressable quantum dot qubit with fault-tolerant control-fidelity, Nat. Nanotechnol. **9**, 981 (2014).

[37] Y. Zeng, P. Xu, X. D. He, Y. Y. Liu, M. Liu, J. Wang, D. J. Papoular, G. V. Shlyapnikov, and M. S. Zhan, Entangling Two Individual Atoms of Different Isotopes via Rydberg Blockade, Phys. Rev. Lett. **119**, 160502 (2017).